Drake Passage and palaeoclimate

J. R. TOGGWEILER[1,*] and H. BJORNSSON[2]
[1]GFDL/NOAA, P.O. Box 308, Princeton, NJ 08542, USA
[2]Atmospheric and Oceanic Sciences Program, Princeton University, P.O. Box CN710, Princeton, NJ 08544, USA

ABSTRACT: The effect of Drake Passage on the Earth's climate is examined using an idealised coupled model. It is found that the opening of Drake Passage cools the high latitudes of the southern hemisphere by about 3°C and warms the high latitudes of the northern hemisphere by nearly the same amount. This study also attempts to determine whether the width and depth of the Drake Passage channel is likely to be an important factor in the thermal response. A deeper channel is shown to produce more southern cooling but the magnitude of the effect is not large. Channel geometry is relatively unimportant in the model because of a haline response that develops when the channel is first opened up. Published in 2000 by John Wiley & Sons, Ltd.

Journal of Quaternary Science

Introduction

South America and Australia separated from Antarctica between 20 and 40 million years ago, isolating Antarctica and the South Pole behind a continuous band of ocean water. The palaeoceanographic record shows that this separation led to the accumulation of glacial ice on Antarctica and an abrupt cooling of the ocean's deep water (Kennett, 1977). Both effects persist to this day. The palaeoceanographic record gives every indication that the isolation of Antarctica was a major step in climate evolution.

Today, the band of open water around Antarctica is most restricted between the tip of South America and the Palmer Peninsula, a feature known as Drake Passage. In one of the earliest scientific papers written about the output of an ocean general circulation model, Gill and Bryan (1971) showed how a gap such as Drake Passage alters the ocean's meridional circulation and heat transport. With Drake Passage closed, the ocean transports heat southward by moving warm water poleward near the surface. Cooling at the Antarctic margin leads to deep-water formation and the northward flow of cold water at depth. With Drake Passage open, warm upper ocean water from the north is unable to flow into or across the channel because there is no net east–west pressure gradient to balance the effect of the Earth's rotation. The ocean's ability to transport heat southward is thereby diminished. Cox (1989), England (1992) and Mikolajewicz et al. (1993) carried out similar experiments with more realistic continental geometries and forcing.

* Correspondence to: J. R. Toggweiler, GFDL/NOAA, P.O. Box 308, Princeton, NJ 08542, USA.
E-mail: jrt@gfdl.gov

The models used in the work cited above were ocean-only models in which the same restoring boundary conditions were applied both before and after Drake Passage was opened. Thus, the circulation is allowed to change but temperatures and salinities at the surface are basically fixed. This strategy implicitly assumes that changes in atmospheric forcing are limited to small departures from the present forcing. Mikolajewicz et al. (1993) computed the change in ocean–atmosphere heat flux implied by the change in circulation and fed the altered heat fluxes into an atmospheric energy balance model to determine how atmospheric temperatures might be expected to change. Perhaps not surprisingly, Mikolajewicz et al. (1993) found that the thermal effect of Drake Passage is very modest. They predicted an 0.8°C cooling (zonally averaged) at 50°S and even smaller temperature changes elsewhere. Mikolajewicz et al. (1993) concluded that their results offer only limited support for the idea that the opening of Drake Passage led to substantially colder conditions on and around Antarctica.

In the present paper we take up the task of opening Drake Passage in a coupled model in which there is no restoration to modern boundary conditions, either before or after Drake Passage is opened. Changes in atmospheric temperatures are not limited to small departures from present temperatures. Salt is free to move within the ocean in response to changes in the circulation.

The channel of open water in the latitude band of Drake Passage has gradually widened and deepened over millions of years. It would not be unreasonable to suppose that Antarctica should become progressively colder in response to the gradual widening and deepening of the channel. Oxygen isotope records, on the other hand, indicate that the initial cooling of Antarctica was rather abrupt (Kennett and Shackleton, 1976). In order to examine the effect of channel geometry, the coupled model was run with shallow (750 m) and deep (2750 m) topographic obstructions within

the channel. The model with shallow obstructions is intended to represent an early phase in the opening of the channel, whereas the model with deep obstructions is intended to represent a late phase.

A water planet model

The model used in this paper describes a water-covered earth in which land is limited to two polar islands and a thin barrier that extends from one polar island to the other. The polar islands cover each pole out to 76.5° latitude, which is roughly the latitude of the Weddell and Ross Sea embayments on Antarctica's perimeter. Figure 1 shows a schematic of the model's land–sea configuration with a segment of the barrier (Drake Passage) removed near the south polar island. The barrier between the polar islands is very thin, 7.5° of longitude wide, or 2% of a latitude circle.

The coupled model consists of a three-dimensional ocean general circulation model coupled to a one-dimensional energy balance model of the overlying atmosphere. As in other coupled models, the model used here finds a latitudinal temperature distribution in which the flux of outgoing long-wave energy is in balance with a specified input of short-wave solar energy. The model does not have interactive winds or an interactive hydrological cycle. Instead, a latitudinally varying wind stress field is imposed on the ocean along with a latitudinally varying salt flux. No attempt is made to include an ice-albedo feedback due to snow cover or ice on the polar islands. There is no sea ice on the ocean.

The atmospheric model, loosely based on the model of North (1975), was provided by I. Held (personal communication). It solves a one-dimensional equation describing the latitudinal variation of the atmospheric heat budget

$$C_p \cdot \frac{\partial T_a}{\partial t} = Q_a \cdot s(\phi) + I + \gamma \cdot (T_o - T_a) \quad (1)$$

$$- (A + B \cdot T_a) + \frac{D}{\cos\phi} \frac{\partial}{\partial \phi} \left(\cos\phi \frac{\partial T_a}{\partial y} \right)$$
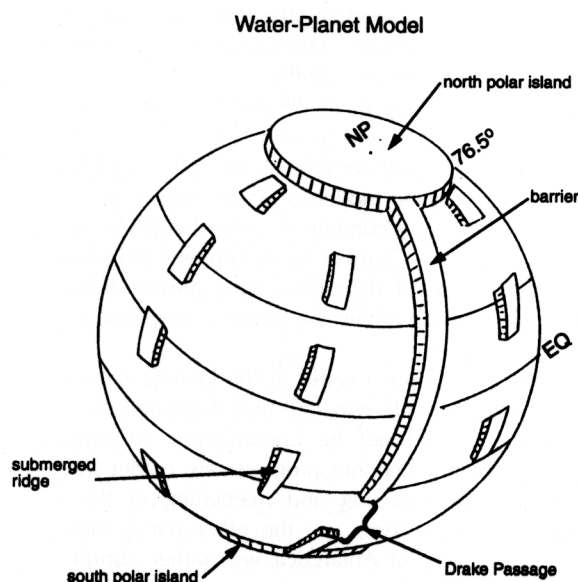
Water-Planet Model

Figure 1 Schematic diagram illustrating the major features of the water planet coupled model.

The corresponding heat balance for the surface layer of the ocean is given by

$$C_o \cdot \frac{\partial T_o}{\partial t} = Q_o \cdot s(\phi) - I - \gamma \cdot (T_o - T_a) + \text{circulation effect} \quad (2)$$

In equations (1) and (2) Q_a and Q_o represent the globally averaged shortwave solar energy absorbed by the atmosphere and ocean, 70 W m^{-2} and 170 W m^{-2}, respectively. The Q_a and Q_o values are multiplied by $s(\phi)$, a function that distributes the incoming shortwave solar energy as a function of latitude. The value of $s(\phi)$ is equal to $1 + 0.7(\cos^2(\phi) - 2/3)$, which averages to unity over a sphere. The earth's albedo is assumed to be uniform and is taken into account by the fact that Q_a and Q_o sum to 240 W m^{-2}, a figure that is 30% lower than the globally averaged shortwave flux at the top of the atmosphere. Variable I is the net longwave energy from the ocean absorbed by the atmosphere (70 W m^{-2}), assumed to be constant with latitude.

The atmosphere radiates longwave energy to space as $A + B \cdot T_a$, where $A = 210$ W m^{-2} and $B = 2$ W m^{-2} deg^{-1}. It transports heat poleward by simple diffusion according to a diffusion parameter D (= 0.30 W m^{-2} deg^{-1}). Parameter D is derived from $kC_pR_e^2$, where k is a diffusion coefficient (= 1.22 × 10^6 m^2 s^{-1}) and R_e is the radius of the earth. In equation (1), C_p is the heat capacity at constant pressure of an entire column of air, 1×10^7 J m^{-2} deg^{-1}. In equation (2), C_o is the heat capacity of the ocean model's 57 m surface layer, 2.3 × 10^8 J m^{-2} deg^{-1}. An exchange coefficient γ (= 30 W m^{-2} deg^{-1}) parameterises the exchange of sensible and latent heat between the ocean and atmosphere in response to the zonally averaged ocean–atmosphere temperature difference.

The atmospheric model is discretised into 40 grid cells, which are aligned with the meridional grid in the ocean. Each atmospheric grid cell exchanges heat with all ocean grid cells in the same latitude band. The heat balance over the thin barrier is ignored. The land surface over the polar islands is assumed to have zero heat capacity. Any heat reaching the surface is released immediately to the atmosphere. Hence, Q_a is set equal to 240 W m^{-2} and both Q_o and I are set equal to 0.

The ocean model is based on the GFDL (Geophysical Fluid Dynamics Laboratory) MOM (Modular Ocean Model) 2 code and is built on a coarse grid (4.5° latitude by 3.75° longitude with 12 vertical levels). The maximum depth is 5000 m. Drake Passage in these experiments is quite wide, extending from 42.75° to 65.25°S. The rationale for such a wide gap is based on the fact that the Antarctic Circumpolar Current (ACC) in coarse models tends to be strongly influenced by lateral friction near the tip of South America. A wide gap helps eliminate lateral friction as a leading order term in the momentum budget for the water planet's ACC.

The ocean floor is mostly flat except for a series of submerged ridge segments that extend up from the bottom. The ridge segments are staggered across the ocean floor as shown in the top panel of Fig. 2. Pressure gradients across the submerged ridges take up >90% of momentum added to the ocean by the wind in the latitude band of Drake Passage; lateral friction takes up <10%. In the first set of model runs, the ridge segments are raised up to 742 m below the surface (the base of model level 5). In the second set of model runs, the ridge tops are deepened to 2768 m (the base of level 9). A ridge depth of 2768 m is characteristic of some of the major topographic obstacles that the modern ACC encounters, including the sill in Drake Passage itself.
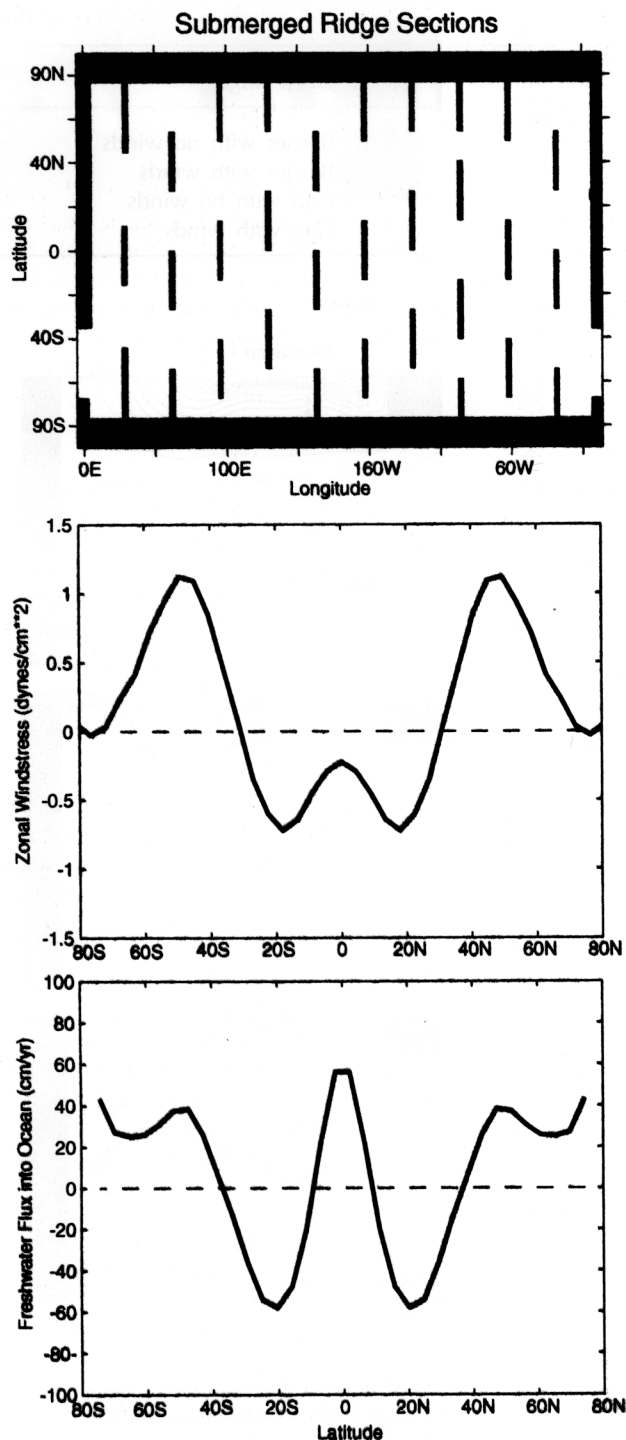
Submerged Ridge Sections

Figure 2 (a) Map of ocean bathymetry showing the positions of submerged ridge segments. (b) Wind stresses imposed on the ocean as a function of latitude. (c) Salinity fluxes imposed on the ocean as a function of latitude, shown as an equivalent freshwater flux in cm yr^{-1}.

The grid and parameter set used to run the ocean model are derived from Toggweiler *et al.* (1989). The model uses a modified version of the Bryan and Lewis (1979) vertical mixing scheme in which vertical mixing varies with depth from 0.15 cm^2 s^{-1} in the upper kilometre to 1.3 cm^2 s^{-1} in the lower kilometre. The model includes the Gent–McWilliams (GM) parameterisation for tracer mixing as implemented in MOM by Griffies (1998). The coefficients governing GM thickness mixing and diffusion along isopycnals have both been set to 0.6 × 10^7 cm^2 s^{-1}. The model uses flux-corrected transport (FCT) to advect tracers, rather

than centred differences, and has no background horizontal mixing. There is no freezing point limitation on the temperatures generated by the model, i.e. ocean temperatures are allowed to fall below −2°C.

The wind forcing on the model is based on the annual-mean wind-stress climatology of Hellerman and Rosenstein (1983). Zonal wind stresses in Hellerman and Rosenstein were averaged first around latitude circles. Northern and southern stresses at the same latitude were then averaged to create a wind-stress field that is symmetric between the hemispheres. The salinity forcing used by the model is derived from the surface water balance (precipitation + runoff − evaporation) determined during the spin-up of the GFDL R30 coupled model (Knutson and Manabe, 1998). The net water flux was first converted to an equivalent salt flux and zonally averaged. It was then averaged between the hemispheres to create a forcing field that is hemispherically symmetric like the wind field. Wind stresses and water fluxes used to force the ocean are plotted as a function of latitude in the middle and bottom panels of Fig. 2.

The coupled model has been used to generate the eight solutions identified in Table 1. Four solutions were generated with a closed gap or full barrier. Four were generated with an open Drake Passage gap. Four of the eight solutions were run out with ridge tops at 742 m, and four with the ridges at 2768 m. Each combination of gap/no gap and shallow/deep ridges was also run out with and without wind forcing. Each solution has been run out for 5000 yr. Selected models in Table 1 have been run as temperature-only models without any salinity forcing.

The next section begins with simulations 2 and 4, the models with shallow ridges and wind forcing, and later considers the models with deep ridges and wind forcing (simulations 6 and 8). Models with no wind forcing are considered in the section following the next. The results from the next two sections are then summarised in terms of the air temperature changes that result from the opening of Drake Passage.

The Drake Passage effect with wind forcing

Zonally averaged temperatures, zonally averaged salinities and the meridional overturning are shown in Fig. 3 for simulation 2, the full barrier model with shallow ridges. The temperature section in the top panel shows that the coupled model produces a reasonable range of surface temperatures, with 0° water next to both polar islands and 28° water on either side of the equator. The coldest water next to the polar islands is found within a shallow halocline produced by the excess of precipitation over evaporation poleward of 40° latitude. Surface water adjacent to the polar islands has a salinity of 33.4 psu in both hemispheres. Deep water below 2000 m is about 0°C, with a salinity just below 34.6 psu. Distributions of temperature and salinity in simulation 2 are more-or-less symmetric about the equator as one would expect from the geometry and forcing of the full barrier models. There is a slight asymmetry in the distributions of temperature and salinity at depth.

The overturning streamfunction in the bottom panel of Fig. 3 includes four wind-driven cells near the surface, which correspond to the easterly and westerly wind bands in Fig. 2. There are two thermally driven cells in the interior with sinking motions next to the two polar islands. The over-

Table 1 Simulations carried out with the water planet model

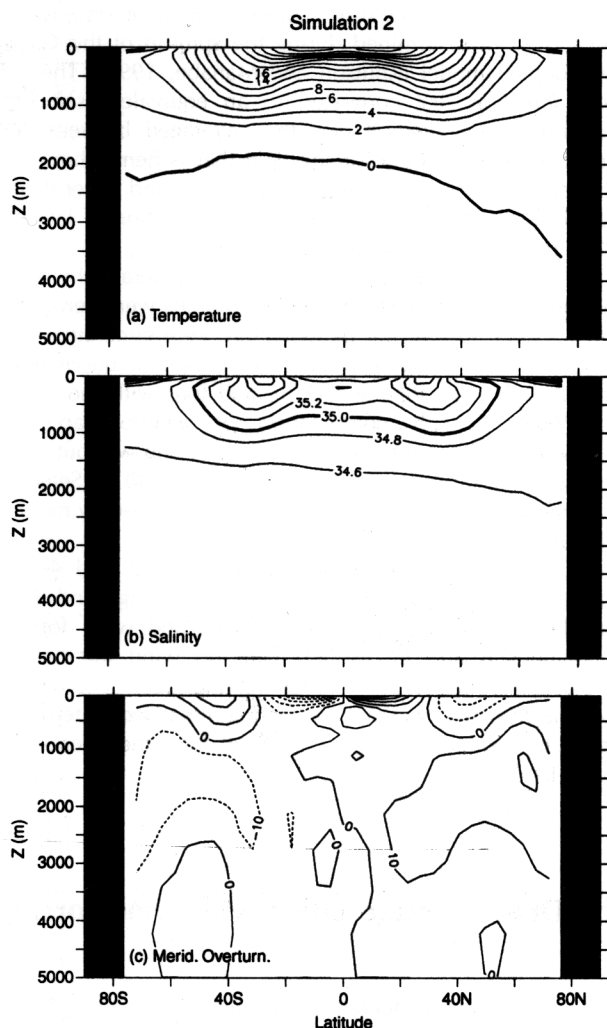| Simulation number	Shallow ridges	Simulation number	Deep ridges
1	Barrier with no winds	5	Barrier with no winds
2	Barrier with winds	6	Barrier with winds
3	Gap with no winds	7	Gap with no winds
4	Gap with winds	8	Gap with winds

Figure 3 Meridional sections through the ocean showing (a) zonally averaged temperatures, (b) zonally averaged salinities and (c) the meridional overturning from the shallow ridges model with a full barrier between the polar islands (simulation 2). The model used to produce these results includes the effect of winds. The 0°C isotherm and the 34.0 and 35.0 psu isopleths of salinity are plotted as bold contours. The meridional overturning is a stream function with units of Sv (= 10^6 m^3 s^{-1}) derived from the zonally integrated meridional and vertical flow. The effect of the Gent–McWilliams parameterisation on tracers is not included. Dashed contours indicate overturning in a counter-clockwise direction.

Figure 4 Same meridional sections shown in Fig. 3 but for the shallow ridges model with a Drake Passage gap (simulation 4). The depth and latitudinal extent of the gap is shaded. The dashed contour next to the south polar island in the temperature section is the −2°C isotherm.

turning in the interior is slightly asymmetric about the equator, with 15–20 Sv of sinking next to each polar island.

The same sequence of results is shown in Fig. 4 for simulation 4 with an open Drake Passage gap. The depth and position of the gap is indicated by shading. Opening Drake Passage with shallow ridges produces a notable shift in surface temperatures, a result that will become more apparent in the next-but-one section. Water next to the south
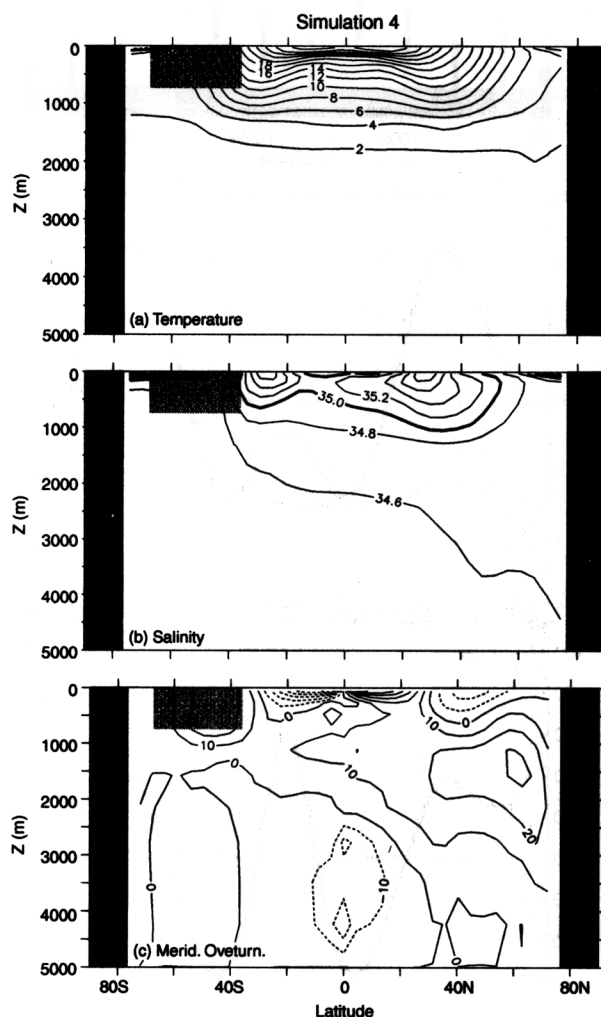
polar island cools to less than −2°C, whereas water next to the north polar island warms to more than +2°C. The outcrop positions of the 2–18°C isotherms are compressed northward away from the south polar island but expand northward up to the polar island in the north. Individual isotherms are found at greater depths, such that water in the interior is about 2°C warmer at a given depth with the open gap. Water next to the north polar island is saltier than water next to the south polar island by 0.2 psu at a depth of 1000 m. The halocline next to the south polar island is considerably more intense, with a minimum salinity at the surface of 32.8 psu. The outcrop position of the 34.0 psu isopleth pushes out to 45°S compared with 65°S in Fig. 3.

The overturning in the bottom panel of Fig. 4 is very

asymmetric, with 30 Sv of sinking next to the north polar island, and virtually no sinking in the south. Streamlines tracking sinking at the north polar island extend across the equator in the upper 2000 m. Some of the water sinking at the north polar island flows all the way to the gap, where it upwells to the surface as part of the Ekman divergence south of 50°S. Some of the water pushed downward by the Ekman convergence in the northern part of the gap then flows all the way up to the region of deep-water formation next to the north polar island. The wind-driven overturning cell in the latitude band of the gap extends downward to a depth just below the level of the ridge tops.

Results from the full barrier model with deep ridges (simulation 6) are shown in Fig. 5. As before, 0°C water is found at each polar island and 28°C water straddles the equator. Isotherms in the lower thermocline are a bit deeper with deep ridges. Deep water in the interior is slightly warmer. The results of simulation 6 are otherwise almost identical to the results of simulation 2; the submerged ridges have very little effect when there is no gap.

Figure 6 shows the same sequence of figures for the deep ridges model with an open gap (simulation 8). As in Fig. 4, the depth and position of the gap is indicated by shading. The surface water next to the south polar island cools to

−4°C, whereas water in the interior becomes significantly warmer. The strength of the ACC increases from 60 Sv in the shallow ridges model to 180 Sv in the deep ridges model. This is reflected in the fact that the thermal contrast across the ACC is larger with deep ridges. Individual isotherms are substantially deeper than in the full barrier case in Fig. 5. Thermocline water is as much as 4°C warmer at a given depth with an open gap and deep ridges.

Simulation 8 with deep ridges produces a salinity minimum layer just north of the channel in which relatively fresh water with polar surface properties penetrates northward at intermediate depths. A salinity minimum is, of course, a prominent feature of the real ocean. A salinity minimum is not seen in the shallow ridges model or in any of the full barrier models, where salinities decrease monotonically to the bottom. Salinities in the upper 1500 m tend to be lower overall in the model with deep ridges, whereas salinities at depth are about 0.1 units higher.

With deep ridges there is a conspicuously stronger north–south circulation linking the wind-driven overturning in the southern channel with the overturning in the northern hemisphere. The flow of southern water northward at intermediate depths is some 10 Sv stronger and the overall sinking rate in the northern hemisphere is also about 10 Sv stronger. These features of the deep ridges model—a northward penetration of relatively fresh intermediate-depth water, and a strong transequatorial overturning circulation—are hallmarks
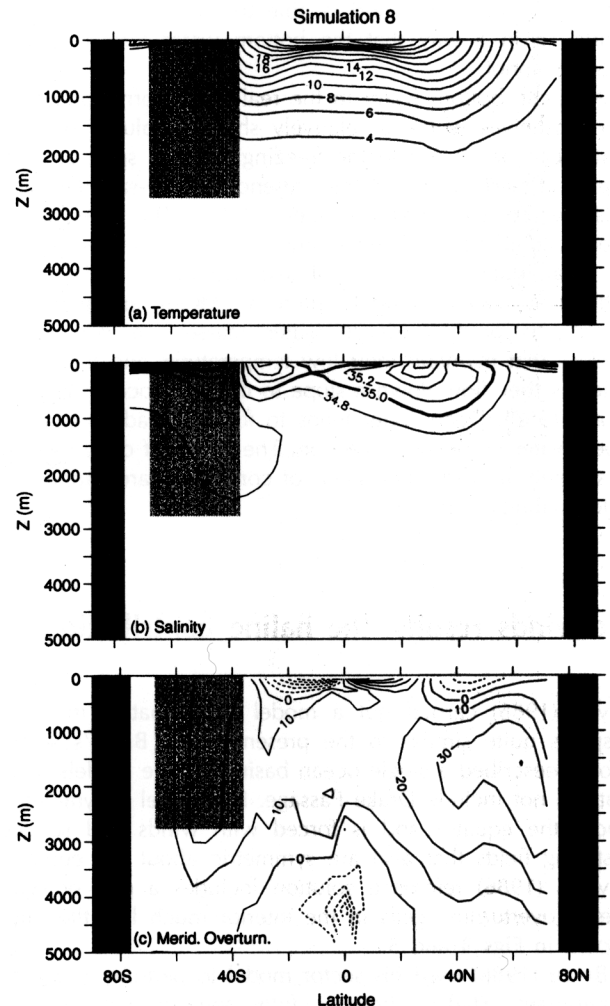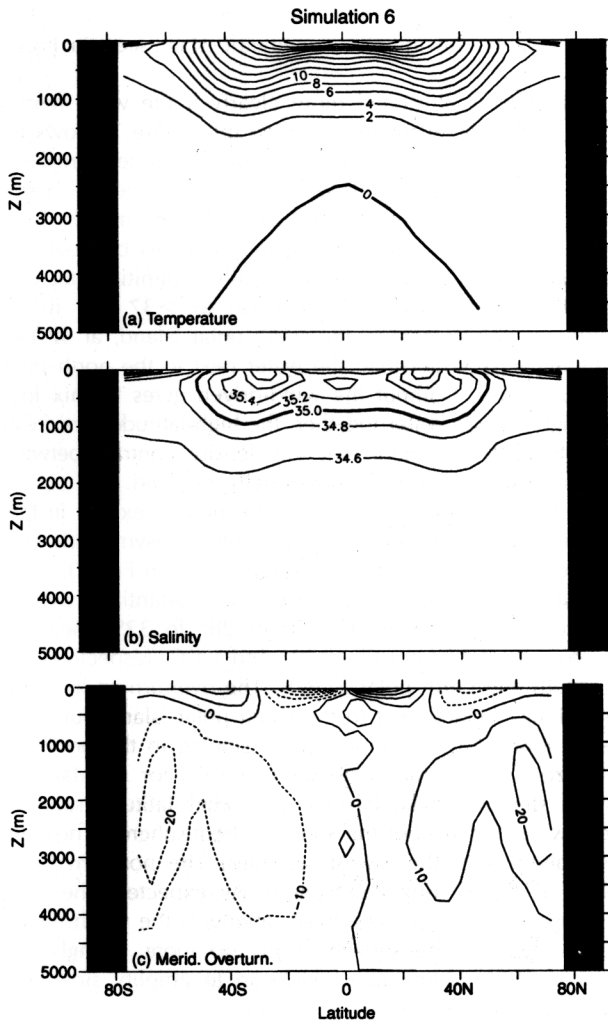

Figure 5 Meridional sections through the ocean showing (a) zonally averaged temperatures, (b) zonally averaged salinities and (c) the meridional overturning from the deep ridges model with a full barrier (simulation 6) including the effect of winds. These results are very similar to results in Fig. 3 from the shallow ridges model.

Figure 6 Same meridional sections shown in Fig. 5 but for the deep ridges model with a Drake Passage gap (simulation 8). The depth and latitudinal extent of the gap is shaded.

of the conveyor circulation in the modern Atlantic (Broecker, 1991). These features appear here as a consequence of an open Drake Passage with deep ridges.

One of the clearest palaeoceanographic changes associated with the separation of Australia and South America from Antarctica is a pronounced cooling of the deep ocean. Kennett and Shackleton (1976) reported a sharp drop in deep-water temperatures of 4–5°C in the circumpolar region when the tectonic isolation of Antarctica began in the early Oligocene. The increased frequency of erosional hiatuses in deep-sea cores at the same time led Kennett and Shackleton (1976) to conclude that a dense Antarctic bottom water also began to be produced at about this time. The model results seen thus far are not consistent with this evidence: bottom-water temperatures tend to warm with the opening of Drake Passage rather than cool, and the meridional overturning initiated in the south becomes weaker rather than stronger.

This feature of the water planet results is likely to be a model artefact. Simulations 6 and 8 were rerun as temperature-only models without any salinity forcing. The temperature-only version of simulation 8 produces a southern bottom water that is 2°C colder than its full-barrier counterpart. Colder surface temperatures associated with the open gap extend directly into the deep ocean instead of being confined to a polar halocline. The northward flow of bottom water away from the south polar island is also dramatically stronger. The temperature-only result described here and the palaeoceanographic observations of Kennett and Shackleton (1976) lead us to suspect that the Antarctic bottom water forming in the real world is able to circumvent the polar halocline in a way that the bottom water formed in the model cannot.

Antarctic bottom water in the real world forms on continental shelves where a relatively shallow volume of shelf water can be cooled to the freezing point in spite of local inputs of freshwater and the presence of low-salinity water offshore (Toggweiler and Samuels, 1995a). The water planet model could be modified easily to include shelves around its polar islands, but model shelves would not make much difference. Ocean models such as MOM are generally unable to produce dense water masses on continental shelves that maintain their low temperatures and high densities as they flow down a slope to the deep ocean (Winton et al., 1998). Deep water tends to form instead in areas of open water by deep convection. The extent of deep cooling is severely limited when areas of convection are capped by a low-salinity halocline.

No-winds results: the haline contribution

Bryan (1986) carried out a model study that is in some respects quite similar to the present study. Bryan's sector model described a single ocean basin, like the models here, but did not include Drake Passage. His model is symmetric about the equator and is forced with winds and surface restoring fields that also are symmetric about the equator. Bryan's (1986) reference solution includes a pair of symmetric overturning cells in the interior much like the ones shown in Figs 3 and 5.

Bryan (1986) used his sector model to perform a famous experiment. Starting from a fully spun-up solution, he removed his restoring boundary condition for salinity and replaced it with a symmetric salt flux that he had diagnosed from his salinity restoring operation. Bryan (1986) then continued his integration using the salt flux. After a few hundred years, the symmetric overturning in Bryan's reference state spontaneously flipped into an asymmetric pole-to-pole overturning in which all deep-water formation shifted into one hemisphere. Salinities rose in the sinking hemisphere and an intense halocline developed in the opposite hemisphere. The shift of salt into the sinking hemisphere ultimately led to a more stable density configuration, with denser water near the bottom and lighter water near the surface. Bryan's (1986) experiment is often cited as an example of how haline effects are able to alter the ocean's overturning circulation because there is no atmospheric feedback to maintain ocean salinities near any particular values.

These same haline effects are at work in the water planet model in a slightly different form. The water planet model has a thermally interactive atmosphere instead of a simple restoring boundary condition. If a symmetric circulation in the water planet model tries to flip into an asymmetric state, temperatures rise in the sinking hemisphere. Warmer temperatures negate the density increase brought about by higher salinities. This effect is strong enough to stabilise the symmetric overturning in the full-barrier simulations 1 and 5 (Figs 3 and 5). A model with a Drake Passage, on the other hand, has a built-in source of asymmetry. Sinking at the south polar island is suppressed by the open gap. Salinities begin to fall in the south and rise in the north. Bryan's (1986) haline effect then comes into play to shift the circulation toward the asymmetric state seen in Figs 4 and 6.

This point is illustrated more clearly if the wind forcing in the water planet model is turned off. Figure 7 shows the standard set of results (zonally averaged temperatures, salinities and the meridional overturning) from the full-barrier model with shallow ridges (simulation 1). The middle panel shows that without winds, the salinity contrast between low and high latitudes grows dramatically. Salinities decrease near the polar islands and increase to >37 psu in the subtropics. Water next to the south polar island, at 32 psu, is significantly saltier than the water next to the north polar island, 29 psu. Without the wind-driven gyres to mix low- and high-latitude water together, the high-latitudes are freshened to such an extent that the density contrast between low and high latitudes is substantially reduced.

The high latitudes are freshened to such an extent, in fact, that the overturning circulation flips into an asymmetric state despite the thermal feedback (bottom panel in Fig. 7). Without winds the ocean's heat transport is substantially weaker. Surface temperatures increase from 28° to 32°C near the equator and cool from 0° to –2° and –4°C, respectively, at the south and north polar islands. The overturning in simulation 1 has sinking next to the south polar island but could just as easily have developed with sinking in the north.

Figure 8 shows the same set of results for simulation 3 with a shallow Drake Passage gap. High-latitude salinities are low, as before, but the southern hemisphere is now the hemisphere with the lowest salinities. The northern hemisphere is the sinking hemisphere. As expected, the open gap suppresses the possibility of sinking in the south. Freshwater added to the surface builds up more strongly and Bryan's (1986) haline effect kicks in to amplify sinking in the north.

Figures 7 and 8 were taken from no-winds models with shallow ridges. Results from the no-winds models with deep ridges are essentially the same. This indicates that the tendency of Bryan's (1986) haline effect to alter the circulation is more-or-less independent of the depth of the gap. This is not unexpected as the gap activates the haline effect by
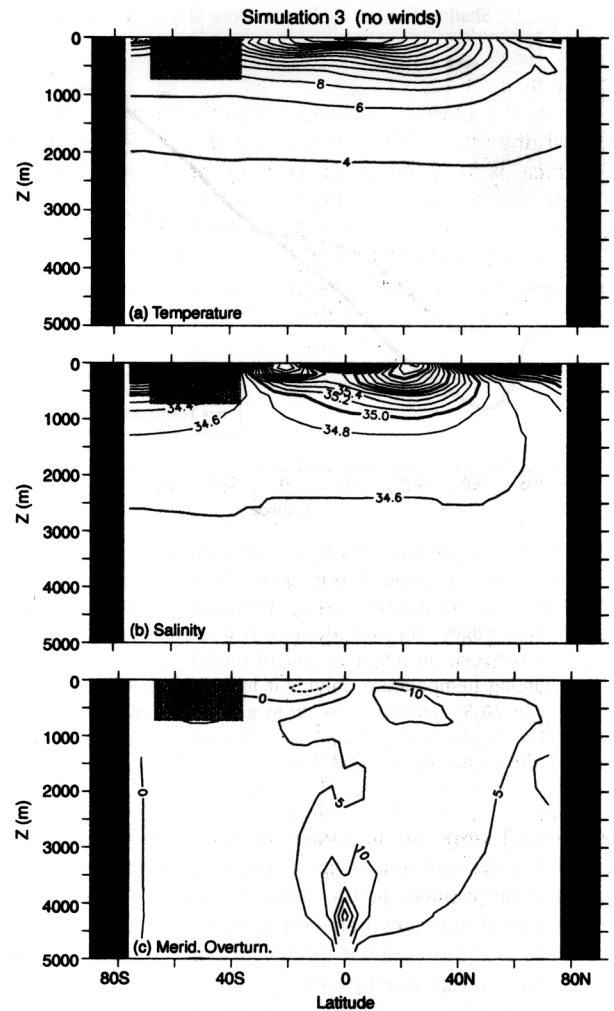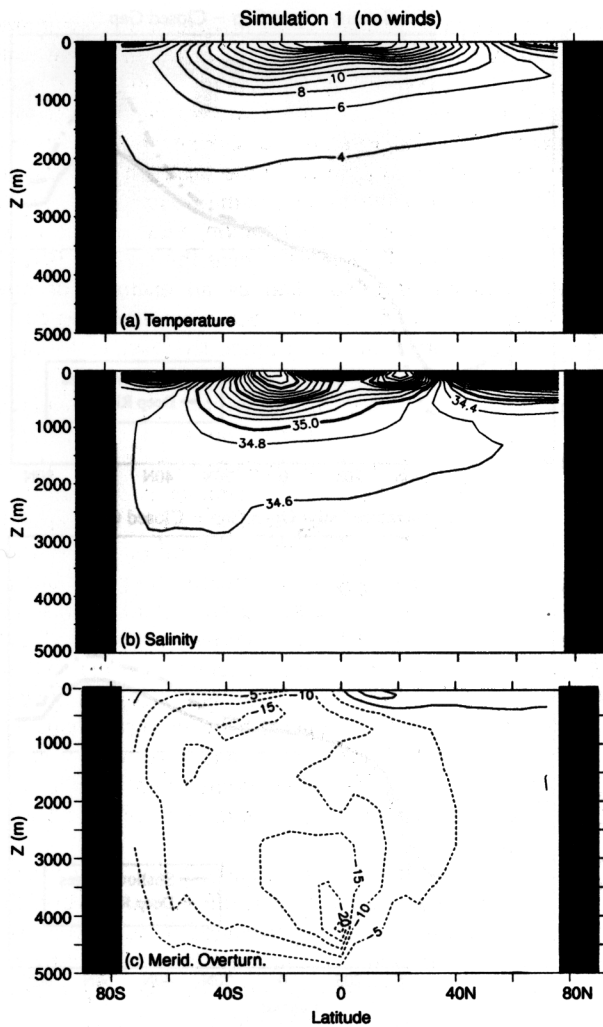
Figure 7 Meridional sections through the ocean showing (a) zonally averaged temperatures, (b) zonally averaged salinities and (c) the meridional overturning from the full barrier model with no winds (simulation 1). Salinity differences are much larger than in Figs 3–6. Bold contours highlight salinity isopleths at 1 psu intervals. Overturning in the no-winds models reaches a quasi-equilibrium state after a few thousand years but still exhibits some variability. The results in Fig. 7 represent an average of six snapshots taken at 250-yr intervals between model years 4000 and 5250.

Figure 8 Same meridional sections shown in Fig. 8 but for the shallow ridges model with a Drake Passage gap and no wind forcing (simulation 3). The depth and latitudinal extent of the gap is shaded. The three results in Fig. 8 represent an average of six snapshots taken at 250-yr intervals between model years 4000 and 5250.

blocking the possibility of sinking in one hemisphere relative to the other. A very narrow gap should be able to carry out this role as well as a very wide gap.

Air temperature differences due to Drake Passage

Surface temperatures in the model with no winds and a full barrier (simulation 1) are warmer in the southern hemisphere, where sinking occurs, than in the northern hemisphere (Figure 7). Surface temperatures in the model with an open gap (simulation 3) are warmer in the northern (sinking) hemisphere (Fig. 8). The same asymmetries are present in the overlying atmosphere. The solid line in Fig. 9 is a plot of the difference in air temperatures between simulation 3 and simulation 1. It shows that air temperatures are cooler everywhere south of the equator and warmer everywhere

north of the equator after the overturning flips from southern sinking in simulation 1 to northern sinking in simulation 3. The air temperature differences in Fig. 9 become quite large, ca. 3°C, next to the polar islands.

The temperature differences given by the solid line in Fig. 9 are the combined effect of two factors. One is the haline effect that causes the overturning to flip from south to north when the gap is opened. The other effect is the ability of Drake Passage to block the overturning in the gap hemisphere. The dotted line in Fig. 9 shows the air temperature differences between an identical pair of no-winds models that were run without salinity forcing. These differences reflect only the tendency of the gap to block the overturning in the southern hemisphere. In this case temperatures near the south polar island cool by only 1.0–1.5°C. The northern hemisphere and the southern hemisphere north of 20°S warm by 0.5°C on average. The relatively uniform warming north of 20°S is a response to the lower temperatures south of 30°S. A reduced flux of outgoing longwave radiation in the far south forces the rest of the planet to warm up slightly to compensate.

The contrast between the two curves in Fig. 9 shows that the haline contribution to gap-induced temperature changes is potentially quite large. A very relevant question is whether
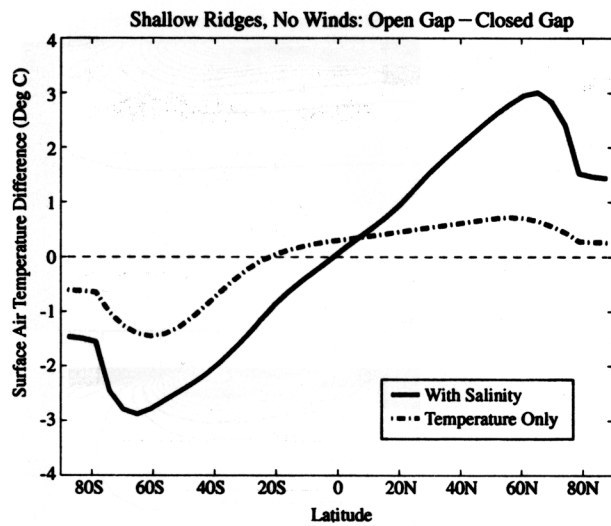
Shallow Ridges, No Winds: Open Gap – Closed Gap

Figure 9 Air temperature differences between no-winds models with and without a Drake Passage gap. The curve plotted with a solid line is T_{air} (simulation 3) − T_{air} (simulation 1) from models with shallow ridges. The dotted curve is the air temperature difference between an identical pair of models run without salinity forcing (temperature only). Air temperature differences poleward of 76.5° latitude come from grid points over the polar islands. The results in Fig. 9 are derived from six snapshots between the model years 4000 and 5250.

the thermal response to Drake Passage can be anywhere near this large without a flip in the overturning circulation from one hemisphere to the other. Figure 10 shows the air temperature differences between wind-forced models where the winds and the coupled model's thermal feedback stabilise the full-barrier overturning. Air temperature differences between simulations 4 and 2 with shallow ridges, and between simulations 8 and 6 with deep ridges, are given in the top panel of Fig. 10. Air temperature differences from temperature-only versions of the same models are given in the bottom panel.

The temperature-only results in the bottom panel of Fig. 10 show that the thermal response to Drake Passage is larger with winds than without. Air temperatures in the model with an open gap and shallow ridges are more than 2°C cooler at 50°–60°S (solid curve), in contrast with the 1.0–1.5°C cooling seen in the no-winds model in Fig. 9. Air temperatures near the north polar island warm by more than 1°C, and there is a distinct shift of the northern warming toward higher latitudes. The enhanced thermal response in the wind-forced models is due to the meridional overturning circulation set up by the westerly winds blowing over the open channel. The winds in the channel draw up cold water from the ocean's interior and force it northward at the surface away from the south polar island. The northward flow takes up solar heat that otherwise would be available to warm the south polar region. The overturning circulation carries this southern heat across the equator into the high latitudes of the northern hemisphere where the southern heat is released to the atmosphere when northern deep water forms.

The water drawn up to the surface in the south comes from greater depths with deeper ridges. This effect increases the temperature difference between the cold water flowing south into the upwelling zone at depth and the warmer water flowing northward at the surface and increases the amount of heat removed from the southern hemisphere. Results in the bottom panel of Fig. 10 show that deep ridges increase the southern cooling due to an open gap by about 1°C. Overall, one sees a fairly regular increase in the
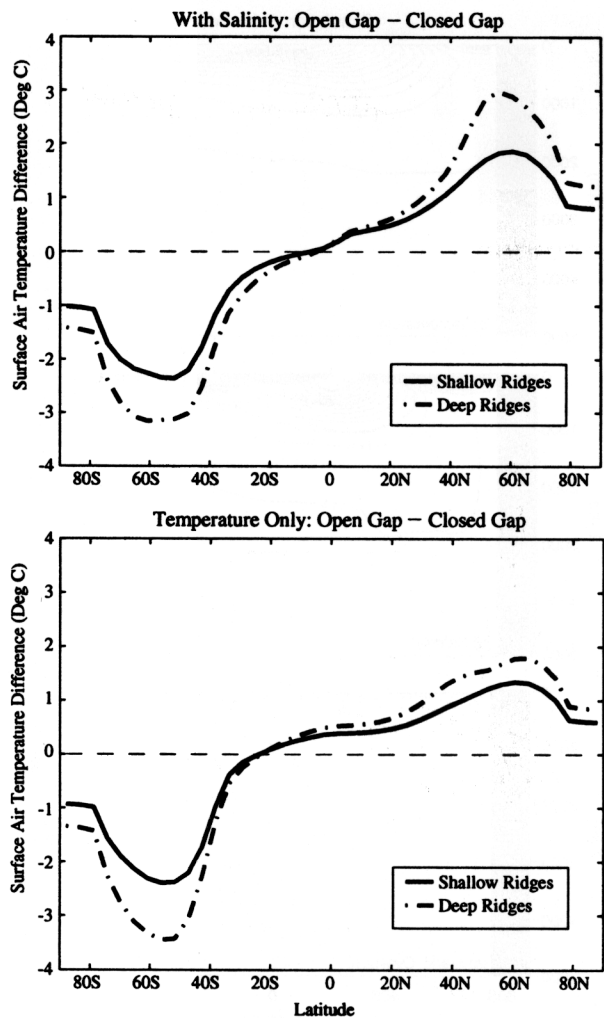
With Salinity: Open Gap – Closed Gap

Temperature Only: Open Gap – Closed Gap

Figure 10 Air temperature differences between wind-forced models with and without a Drake Passage gap. (a) Comparison of air temperature differences in shallow and deep ridges models run with salinity forcing. Solid curve is for models with shallow ridges, T_{air} (simulation 4) − T_{air} (simulation 2). Dashed-dot curve is for models with deep ridges, T_{air} (simulation 8) − T_{air} (simulation 6). (b) Comparison of air temperature differences in the same set of models run without salinity forcing (temperature only).

maximum level of southern cooling with increasing wind effect, 1.4°C with no winds (dotted line in Fig. 9), 2.4°C with winds and shallow ridges, and 3.4°C with winds and deep ridges (solid and dashed lines in the bottom panel of Fig. 10).

The thermal response to an open gap is a bit different with salinity forcing (top panel of Fig. 10). With salinity forcing, the warming associated with deep-water formation next to the north polar island is larger still and is even more concentrated in high latitudes. The main effect of salinity forcing in the south is a narrowing of temperature differences between the shallow and deep ridges models. The maximum level of southern cooling in simulation 8 with deep ridges is reduced by a few tenths of a degree as the cooling effect of the gap broadens into the tropics.

The thermal response to an open gap in the top panel of Fig. 10 is ca. 3°C, mostly because of the wind effect. North–south salinity differences generally seem to enhance the thermal effect of an open Drake Passage. Saltier deep water increases the amount of heat lost from the ocean next to the north polar island and the strength of the interhemispheric conveyor. Of particular interest is the fact that salinity differ-

ences reduce the impact of deep ridges in the south. This result is important because it suggests that an active haline effect makes the thermal response to Drake Passage less dependent on the depth and width of the channel.

Discussion

The model results described here show that the existence of a gap between South America and Antarctica not only cools the Southern Ocean but also warms the high latitudes of the Northern Hemisphere. Cooling in the south and warming in the north are characteristic effects of the trans-equatorial conveyor circulation in the modern Atlantic (Crowley, 1992). The modern conveyor is usually viewed in terms of the special factors that enhance deep-water formation in the North Atlantic (Broecker, 1991), but there are no special factors here: the conveyor simply appears when Drake Passage is opened in the presence of winds.

The winds driving the ACC have been shown to produce a transequatorial conveyor in ocean-only GCMs that is not dependent on diapycnal mixing in the interior (Toggweiler and Samuels, 1995b, 1998). As in the coupled model here, the winds in these models raise cold dense water to the surface around Antarctica and cause it to be warmed and freshened as it moves northward in the surface Ekman layer. This warmer, lighter water is then pumped down into the thermocline north of the ACC, thickening the lower thermocline all the way up to the latitude of Iceland (Gnanadesikan, 1999; Vallis, 2000). The presence of relatively warm water at 500–1000 m enhances the density contrast across the Icelandic sills and thereby enhances the formation of North Atlantic Deep Water. Deep-water formation in the North Atlantic converts warm thermocline water back into cold water that is dense enough to flow southward at depths below the channel's topographic barriers.

It is interesting to note in Fig. 10 that the overturning circulation initiated by an open Drake Passage has very little impact on the magnitude of tropical temperatures. This is because the same volume of cold deep water upwells through the thermocline in low latitudes whether Drake Passage is open or not. A wind-powered conveyor linked to Drake Passage mainly transfers heat from the high latitudes of the southern hemisphere to the high latitudes of the northern hemisphere.

The southern cooling and northern warming produced by an open Drake Passage in the water planet model is of the right magnitude to explain the observed temperature differences between the Northern and Southern Hemispheres. The bold solid curve in Fig. 11 shows the departure of zonally averaged sea-surface temperatures (SSTs) in simulation 8 from the mean SST calculated by averaging the northern and southern hemispheres at each latitude. As with the air temperature differences in Fig. 10, SSTs poleward of 50° latitude are about 3°C warmer in the north and 3°C colder in the south than the interhemispheric mean. This yields a total SST difference, north minus south, of ca. 6°C. The bold dashed curve in Fig. 11 shows SST departures calculated the same way for the Atlantic Ocean using the Levitus (1982) climatology. Peak SST departures in the Levitus data set are found in the 50–60° latitude band and are also about 3°C. The dotted curve in Fig. 11 shows SST departures for the whole ocean. The global SST departures differ from those in the Atlantic basin mainly between 40°
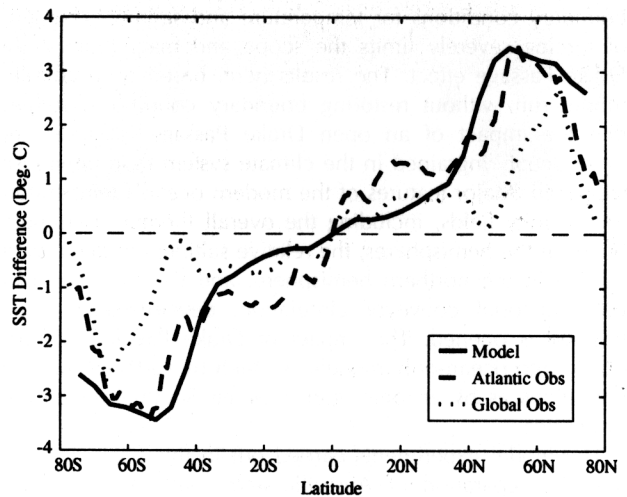
Figure 11 Zonally averaged sea-surface temperature (SST) departures from the mean hemispherically averaged SSTs. The bold solid curve is from simulation 8 (open gap, deep ridges, wind and salinity forcing). The bold dashed curve is derived from observed SSTs in the Atlantic basin. The dotted curve is derived from observed SSTs over the whole ocean. Observed SSTs are taken from the upper 50 m of the Levitus (1982) climatology.

and 50°, where the North Pacific is cooler than the North Atlantic.

Kennett and Shackleton (1976) and Kennett (1977) envisioned that the separation of Antarctica from Australia and South America led mainly to cooler conditions on Antarctica and in the Southern Ocean. They did not note a correlation between southern cooling and northern warming. The situation in the palaeoceanographic record is complicated by the fact that a second globe-encircling seaway was open at the time that Antarctica separated from Australia and South America. The second seaway passed through the Northern Tethys, between Africa and Europe, and between North and South America at latitudes between the Equator and 30°N. It finally closed up when the Arabian Peninsula collided with southern Asia about 15 million years ago in the middle Miocene (Woodruff and Savin, 1989; Flower and Kennett, 1994).

Technically speaking, the full barrier configuration in the water planet model applies only to a time period in the distant past (Triassic) when there was no northern seaway and no Drake Passage (Hsu and Bernoulli, 1978). Similarly, the Drake Passage gap configuration applies only to the last 15 million years when the southern gap is open and the northern seaway has closed up. Preliminary results with the water planet model show that an open channel in the latitude band of the ancient Tethyan seaway is itself very effective at inducing ocean heat transport toward the north polar island. Thus, the opening of a southern gap in a configuration with a pre-existing northern seaway may ultimately cool the south more than it warms the north.

Conclusions

The study of Mikolajewicz et al. (1993) casts doubt on the idea that the opening of Drake Passage is sufficient to account for the magnitude of southern cooling observed in the palaeoceanographic record. However, the Mikolajewicz et al. (1993) study was carried out in a model with restoring

boundary conditions for temperature and salinity. This kind of forcing severely limits the scope and magnitude of the Drake Passage effect. The results here, based on a coupled model run without restoring boundary conditions, suggest that the impact of an open Drake Passage is larger and more deeply ingrained in the climate system than previously supposed. Major features of the modern ocean's temperature and salinity fields, including the overall thermal asymmetry between the hemispheres, the relative saltiness of deep water formed in the northern hemisphere, and the existence of a transequatorial conveyor circulation, develop after Drake Passage is opened. The impact of Drake Passage is introduced into ocean-only models as much by surface boundary conditions as by an open gap between South America and Antarctica.

The model experiments carried out in this paper indicate that the separation of Australia and South America from Antarctica was associated with a ca. 3°C cooling of the air and seas around Antarctica. This level of cooling comes about because of the transequatorial overturning circulation set up by Drake Passage and the westerly winds over the open channel. The upwelling branch of this circulation, forced directly by the westerlies in the south, takes up solar heat that would have been available to warm the polar regions of the Southern Hemisphere. This heat is carried across the equator into the North Atlantic where it is given back to the atmosphere, effectively warming the Northern Hemisphere at the expense of the Southern Hemisphere.

The results here suggest that much of the full thermal effect of Drake Passage could have been realised well before the channel was very wide or very deep. This is because the mere presence of an open gap introduces an asymmetry into the system that is amplified by higher salinities in the north and lower salinities in the south. This kind of haline effect, and the possibility of increased Antarctic sea-ice and land-ice, lead us to conclude that the thermal response to the opening of Drake Passage could have been fairly abrupt and quite large, perhaps as large as the 4–5°C cooling seen in palaeoceanographic observations.

References

Broecker WS. 1991. The great ocean conveyor. *Oceanography*, **4**, 79–89.

Bryan F. 1986. High-latitude salinity effects and interhemispheric thermohaline circulations. *Nature* **323**: 301–304.

Bryan K, Lewis L. 1979. A water mass model of the World Ocean. *Journal of Geophysical Research* **84**: 2503–2517.

Cox MD. 1989. An idealized model of the world ocean, Part I: the global-scale water masses. *Journal of Physical Oceanography* **19**: 1730–1752.

Crowley TJ. 1992. North Atlantic Deep Water cools the southern hemisphere. *Paleoceanography* **7**: 489–497.

England MH. 1993. Representing the global-scale water masses in ocean general circulation models. *Journal of Physical Oceanography* **23**: 1523–1552.

Flower BP, Kennett JP. 1994. The middle Miocene climatic transition: East Antarctic ice sheet development, deep ocean circulation, and global carbon cycling. *Paleogeography, Paleoclimatology, Paleoecology* **108**: 537–555.

Gill AE, Bryan K. 1971. Effects of geometry on the circulation of a three-dimensional southern hemisphere ocean model. *Deep-sea Research* **18**: 685–721.

Gnanadesikan A. 1999. A simple predictive model for the structure of the oceanic pycnocline. *Science* **283**: 2077–2079.

Griffies SM. 1998. The Gent–McWilliams skew flux. *Joournal of Physical Oceanography* **28**: 831–841.

Hellerman S, Rosenstein M. 1983. Normal monthly wind stress over the world ocean with error estimates. *Journal of Physical Oceanography* **13**: 1093–1104.

Hsu KJ, Bernoulli D. 1978. Genesis of the Tethys and the Mediterranean. *Initial Reports of the Deep Sea Drilling Project* **42**: 943–950.

Kennett JP. 1977. Cenozoic evolution of Antarctic glaciation, the circum-Antarctic ocean, and their impact on global paleoceanography. *Journal of Geophysical Research* **82**: 3843–3860.

Kennett JP, Shackleton NJ. 1976. Oxygen isotopic evidence for the development of the psychrosphere 38 Myr ago. *Nature* **260**: 513–515.

Knutson TR, Manabe S. 1998. Model assessment of decadal variability and trends in the tropical Pacific Ocean. *Journal of Climate* **11**: 2273–2296.

Levitus S. 1982. *Climatological Atlas of the World Ocean.* NOAA Professional Report 13, U.S. Government Printing Office: Washington, DC.

Mikolajewicz U, Maier-Reimer E, Crowley TJ, Kim K-Y. 1993. Effect of Drake Passage and Panamanian gateways on the circulation of an ocean model. *Paleoceanography* **8**: 409–426.

North GR. 1975. Analytical solution to a simple climate model with diffusive heat transport. *Journal of Atmospheric Science* **32**: 1301–1307.

Toggweiler JR, Samuels B. 1995a. Effect of sea ice on the salinity of Antarctic bottom waters. *Journal of Physical Oceanography* **25**: 1980–1997.

Toggweiler JR, Samuels B. 1995b. Effect of Drake Passage on the global thermohaline circulation. *Deep-sea Research I* **42**: 477–500.

Toggweiler JR, Samuels B. 1998. On the ocean's large-scale circulation near the limit of no vertical mixing. *Journal of Physical Oceanography* **28**: 1832–1852.

Toggweiler JR, Dixon K, Bryan K. 1989. Simulations of radiocarbon in a coarse-resolution world ocean model, 1, steady state pre-bomb distributions. *Journal of Geophysical Research* **94**: 8243–8264.

Vallis GK. 2000. Large-scale circulation and production of stratification: effects of wind, geometry and diffusion. *Journal of Physical Oceanography* **30**: 933–954.

Winton M, Hallberg R, Gnanadesikan A. 1998. Simulation of density-driven frictional downslope flow in z-coordinate ocean models. *Journal of Physical Oceanography* **28**: 2163–2174.

Woodruff F, Savin S. 1989. Mid-Miocene deepwater oceanography. *Paleoceanography* **8**: 87–140.